NS5 from dengue virus serotype 2 can adopt a conformation analogous to that of its Zika virus and Japanese encephalitis virus homologues

El Sahili, Abbas; Soh, Sherryl Tingjin; Schiltz, Jonas; Gharbi-Ayachi, Aïcha; Seh, Cheah Chen; Shi, Pei-Yong; Lim, Siew Pheng; Lescar, Julien

2019

El Sahili, A., Soh, S. T., Schiltz, J., Gharbi-Ayachi, A., Seh, C. C., Shi, P.-Y., . . . Lescar, J. (2020). NS5 from dengue virus serotype 2 can adopt a conformation analogous to that of its Zika virus and Japanese encephalitis virus homologues. Journal of Virology, 94(1), e01294-19-. doi:10.1128/jvi.01294-19

https://hdl.handle.net/10356/142215

https://doi.org/10.1128/JVI.01294-19

AMERICAN SOCIETY FOR MICROBIOLOGY | Journal of Virology®

STRUCTURE AND ASSEMBLY

NS5 from Dengue Virus Serotype 2 Can Adopt a Conformation Analogous to That of Its Zika Virus and Japanese Encephalitis Virus Homologues

Abbas El Sahili,[a] Tingjin Sherryl Soh,[a,b] Jonas Schiltz,[b,c] Aïcha Gharbi-Ayachi,[a] Cheah Chen Seh,[b] Pei-Yong Shi,[b*] Siew Pheng Lim,[b*] Julien Lescar[a,d]

[a]NTU Institute of Structural Biology, School of Biological Sciences, Nanyang Technological University, Singapore
[b]Novartis Institute for Tropical Diseases, Singapore
[c]Institute of Biochemistry, Center for Structural and Cell Biology in Medicine, University of Lübeck, Lübeck, Germany
[d]Antimicrobial Resistance Interdisciplinary Research Group, Singapore-MIT Alliance for Research and Technology, Singapore

ABSTRACT Flavivirus nonstructural protein 5 (NS5) contains an N-terminal methyltransferase (MTase) domain and a C-terminal polymerase (RNA-dependent RNA polymerase [RdRp]) domain fused through a 9-amino-acid linker. While the individual NS5 domains are structurally conserved, in the full-length protein, their relative orientations fall into two classes: the NS5 proteins from Japanese encephalitis virus (JEV) and Zika virus (ZIKV) adopt one conformation, while the NS5 protein from dengue virus serotype 3 (DENV3) adopts another. Here, we report a crystallographic structure of NS5 from DENV2 in a conformation similar to the extended one seen in JEV and ZIKV NS5 crystal structures. Replacement of the DENV2 NS5 linker with DENV1, DENV3, DENV4, JEV, and ZIKV NS5 linkers had modest or minimal effects on *in vitro* DENV2 MTase and RdRp activities. Heterotypic DENV NS5 linkers attenuated DENV2 replicon growth in cells, while the JEV and ZIKV NS5 linkers abolished replication. Thus, the JEV and ZIKV linkers likely hindered essential DENV2 NS5 interactions with other viral or host proteins within the virus replicative complex. Overall, this work sheds light on the dynamics of the multifunctional flavivirus NS5 protein and its interdomain linker. Targeting the NS5 linker is a possible strategy for producing attenuated flavivirus strains for vaccine design.

IMPORTANCE Flaviviruses include important human pathogens, such as dengue virus and Zika virus. NS5 is a nonstructural protein essential for flavivirus RNA replication with dual MTase and RdRp enzyme activities and thus constitutes a major drug target. Insights into NS5 structure, dynamics, and evolution should inform the development of antiviral inhibitors and vaccine design. We found that NS5 from DENV2 can adopt a conformation resembling that of NS5 from JEV and ZIKV. Replacement of the DENV2 NS5 linker with the JEV and ZIKV NS5 linkers abolished DENV2 replication in cells, without significantly impacting *in vitro* DENV2 NS5 enzymatic activities. We propose that heterotypic flavivirus NS5 linkers impede DENV2 NS5 protein-protein interactions that are essential for virus replication.

KEYWORDS flaviviruses, dengue virus, nonstructural protein, RNA methyltransferase, RNA-dependent RNA polymerase, X-ray crystallography, nonstructural protein 5

Flaviviruses include important human pathogens, such as dengue virus (DENV), Zika virus (ZIKV), and yellow fever virus (1–3). Their genomes encode a highly conserved multifunctional nonstructural protein 5 (NS5) essential for flavivirus RNA replication (4, 5). NS5 contains an N-terminal methyltransferase (MTase) domain and a C-terminal polymerase (RNA-dependent RNA polymerase [RdRp]) domain fused through a poorly

Citation El Sahili A, Soh TS, Schiltz J, Gharbi-Ayachi A, Seh CC, Shi P-Y, Lim SP, Lescar J. 2020. NS5 from dengue virus serotype 2 can adopt a conformation analogous to that of its Zika virus and Japanese encephalitis virus homologues. J Virol 94:e01294-19. https://doi.org/10.1128/JVI.01294-19.

Editor Mark T. Heise, University of North Carolina at Chapel Hill

Address correspondence to Siew Pheng Lim, siewpheng-lim@denka.com.sg, or Julien Lescar, julien@ntu.edu.sg.

* Present address: Pei-Yong Shi, Department of Biochemistry & Molecular Biology, Sealy Center for Structural Biology & Molecular Biophysics, University of Texas Medical Branch, Galveston, Texas, USA; Siew Pheng Lim, Denka Life Innovation Research Pte. Ltd., Nucleos, Singapore.

Received 7 August 2019
Accepted 30 September 2019
Accepted manuscript posted online 9 October 2019
Published 12 December 2019

conserved 9-amino-acid linker (6, 7) that endows the protein with flexibility and enzymatic cooperativity. The MTase domain catalyzes the formation of a type I RNA cap, which is critical for efficient translation and for subverting host immune surveillance (8–10). The RdRp domain synthesizes both negative-strand RNA from the genomic RNA (gRNA) and the progeny plus-strand gRNA (7, 11). Evidence of cross talk or cooperativity between the two enzymatic domains of NS5 was derived from the observation that NS5 exhibits *de novo* initiation (*dn*I) and elongation activities significantly enhanced over those of the RdRp domain alone (12, 13). Due to its functional importance, flavivirus NS5 has been the subject of numerous biochemical, biophysical, and reverse genetics studies for antiviral intervention (14–16). The flavivirus MTase domain (residues 1 to 262) and RdRp domain (residues 272 to 900), either alone (8, 17–20) or in the context of the full-length NS5 protein (20–26), are structurally conserved, yet two classes of flavivirus NS5 conformations have been observed: the NS5 protein from DENV serotype 3 (DENV3) is compact (20–23), while the NS5 proteins from Japanese encephalitis virus (JEV) and ZIKV (24–26) are more open and elongated. This correlates with conformational differences in their interdomain linkers: residues 263 to 266 of the DENV3 linker form a compact 3_{10}-helix (20–23), while ZIKV (24, 25) and JEV (26) linkers are extended and flexible. Consequently, their MTase and RdRp domains have different relative orientations and interdomain interfaces. In solution, the isolated DENV1 to DENV4 NS5 proteins can adopt multiple conformations (27, 28).

RESULTS AND DISCUSSION

Overall structure. To address the question of NS5 conformational variability, we solved the structure of the full-length NS5 protein from DENV2 (residues 1 to 900) using X-ray crystallography. The DENV2 NS5 crystal structure was determined at a resolution of 2.3 Å by molecular replacement (Table 1; see also Materials and Methods). Two molecules per asymmetric unit of the crystal are arranged as a dimer around a noncrystallographic dyad. The two monomers have the same conformation, as they can be superimposed with a residual root mean square deviation (RMSD) of 0.66 Å. Due to mobility, some regions could not be built in monomer A (residues 1 to 6, 464 to 467 [part of motif F], and 885 to 900) and monomer B (residues 1 to 7 and 885 to 900). In all available NS5 structures (20–26), including the structure determined in this work, the MTase domain is located at the back of the RdRp, when the latter is viewed in its front-view orientation (6, 11) (Fig. 1A). In both DENV2 NS5 monomers, the linker is well defined and adopts an extended conformation (Fig. 1A, inset), in contrast to the conformation in DENV3 NS5, where it is more compact (20–23). Thus, DENV2 NS5 has a conformation similar to that of the ZIKV and JEV NS5 proteins (24–26) (Fig. 1B and Table 2). Nevertheless, their conformations are not identical (Fig. 1B and C): following superposition of their RdRp domains, a residual rotation of 17° is needed to overlay the MTase domains of DENV2 and JEV (Fig. 1C). Using the DynDom protein domain motion analysis server, the movement between the MTase and RdRp domains of DENV3 and DENV2 was found to correspond to a hinge motion with respect to the interdomain linker, supporting the role of the linker as a pivot for NS5 dynamics.

DENV2 NS5 forms a head-to-tail noncrystallographic dimer. Like other flavivirus NS5 structures (20–26), DENV2 NS5 forms a head-to-tail dimer (Fig. 2A) with overall molecular dimensions of 80 Å by 90 Å by 70 Å and a central opening of about 20 Å, with several charged residues from the RdRp being exposed at the RNA tunnel entrance (Fig. 2B). The total buried interface is only 1,038 Å^2, which agrees with the observation that the dimer is not stable following gel filtration. However, it is possible that, in the context of the replication complex, NS5 multimerizes (6). Dimeric contacts are formed mainly between the MTase and RdRp domains as well as between the two RdRp domains of adjacent monomers (Fig. 2B and C; see Table 3 for a complete list of the residues involved in monomer-monomer interactions). Compared to DENV3 NS5 dimers (23), DENV2 RdRp domains are shifted with respect to the MTase domains (Fig. 3). The two DENV2 NS5 monomers are arranged such that the MTase RNA binding groove of one DENV2 monomer is oriented toward the RdRp thumb double-stranded RNA exit

TABLE 1 Crystallographic data collection and refinement statistics

Parameter	Value[a]
Wavelength (Å)	0.980105
Resolution range (Å)	55–2.3 (2.44–2.29)
Space group	$P2_1$
Unit cell dimensions	
a, *b*, *c* (Å)	86.68, 146.14, 97.24
α, β, γ (°)	90.0, 105.4, 90.0
No. of measured reflections	401,355 (62,916)
No. of unique reflections	103,117 (16,247)
Multiplicity	3.89 (3.87)
Completeness (%)	99.7 (97.3)
Mean *I*/sigma *I* (*I*)	8.62 (0.97)
R_{merge}[b]	0.105 (1.078)
$R_{measured}$[c]	0.122 (1.252)
$CC_{1/2}$[d]	99.6 (63.1)
R_{work} (%)[e]	19.56
R_{free} (%)[f]	23.45
No. of nonhydrogen atoms	
Macromolecules	14,070
Ligands	80
Water molecules	892
Protein residues	1,751
RMSD	
Bond length (Å)	0.010
Bond angle (°)	1.14
Ramachandran plot (%)	
Favored regions	99.4
Outliers	0.6
Average B factor (Å^2)	
Protein	59.98
SAM[g]	65.04
Solvent	57.84
PDB accession no.	5ZQK

[a]Values for the highest-resolution shell are indicated in parentheses.
[b]$R_{merge} = \sum|I_j - \langle I\rangle|/\sum I$, where I_j is the intensity of an individual reflection, and $\langle I\rangle$ is the average intensity of that reflection.
[c]$R_{measured} = \dfrac{\sum_{hki}\sqrt{\frac{n}{n-1}}\sum_{j=1}^{n}|I_{hkl} - \langle I_{hkl}\rangle|}{\sum_{hkl}\sum_j I_{hklj}}$. *h*, *k*, and *l* are the Miller indices; *n* is the number of measured reflections; and *j* is the *j*th measurement of reflection *hkl*.
[d]$CC_{1/2}$, percent correlation between intensities from a random half of the data set.
[e]$R_{work} = \sum||F_o| - |F_c||/\sum|F_c|$, where F_o denotes the observed structure factor amplitude and F_c denotes the structure factor amplitude calculated from the model.
[f]R_{free} is as for R_{work} but calculated with 5% of randomly chosen reflections omitted from the refinement.
[g]SAM, *S*-adenosylmethionine.

site of the other monomer (Fig. 2B and C). As a result, the distance between residue F25 of one MTase monomer and residue H798 in the RdRp priming loop of the other monomer is 43 Å. Residue F25 stacks capped viral RNA for MTase activity (8, 23), and H798 stacks incoming 5′ ATP during *dn*I of RdRp activity (29) (Fig. 2B). In this arrangement, positively charged patches at the MTase and RdRp template-binding tunnel are exposed to the solvent and are accessible to accommodate incoming RNA substrates for capping and RNA synthesis, respectively. Sequential N-7 and 2′-*O* methylation requires repositioning of the viral RNA substrate (30), a task that could be greatly facilitated by oligomerization of NS5 proteins exchanging RNA substrates. Cooperative dimeric models have already been proposed for NS5 from JEV (26) and DENV3 (21), although with orientations different from the orientation observed here (Fig. 3).

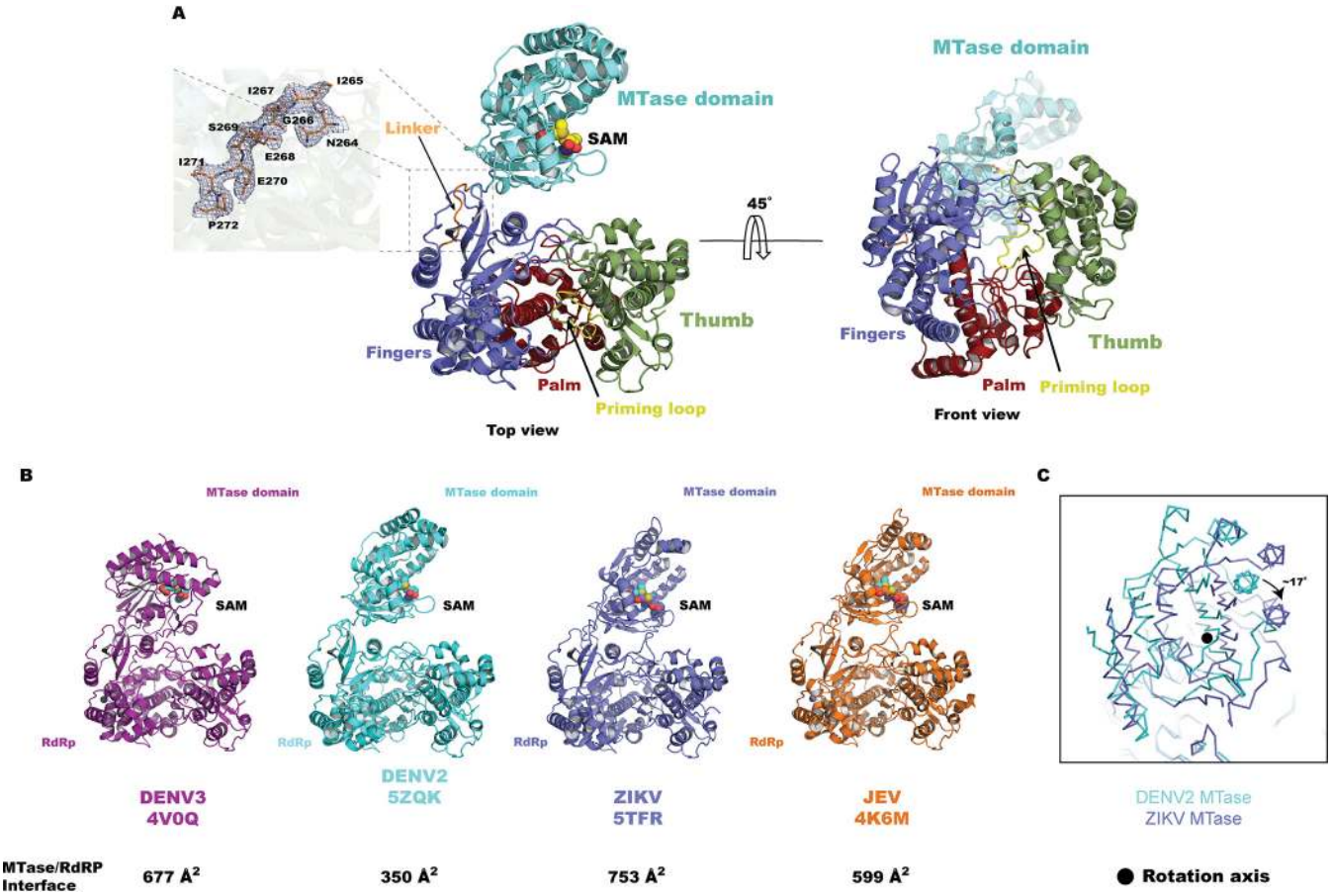

FIG 1 Crystal structure of the full-length NS5 from DENV2. (A) (Left) Overview of the DENV2 NS5 monomer, highlighting its open arrangement, with MTase being colored in cyan and the RdRp subdomains being colored in green (thumb), red (palm), and purple (fingers). The priming loop, which serves as a platform for initiating RNA replication, is colored in yellow and labeled. The linker (orange) connecting the MTase and RdRp domains is extended. Atoms from the bound SAM cofactor are displayed as colored spheres. The inset shows a magnified view of residues N264 to P272 (represented as sticks) from the linker with a $2F_o - F_c$ electron density map (where F_o denotes the observed structure factor amplitude and F_c denotes the structure factor amplitude calculated from the model), contoured at a level of 1σ, overlaid. (Right) A 45° rotation of the image on the left, showing the usual front view of the RdRp domain of NS5. In this orientation, the MTase domain is positioned in the back of the RdRp domain, as was consistently found in all NS5 crystallographic structures determined so far (20–26). (B) Side-by-side comparison of the NS5 monomer from various flaviviruses. All NS5 proteins are shown as colored ribbons, with their RdRp domains being in a common orientation and the SAM cofactor being shown as colored spheres. The respective PDB accession numbers are indicated. The relative orientations of the MTase and RdRp domains range from compact for NS5 from DENV3 (20–23) to open for NS5 from ZIKV (24, 25), JEV (26), and DENV2 (this work). (C) Following superposition of the RdRp domain of NS5 from DENV2 (this work) and from ZIKV (PDB accession number 5TFR), a residual rotation of approximately 17° (about a rotation axis perpendicular to the plane of the figure, represented by a dot) is needed to bring their MTase domains into coincidence.

Regardless of the precise conformation adopted by the NS5 monomer (either compact in DENV3 or extended, as shown here, for DENV2 NS5), the molecular envelope occupied by the full-length dimeric protein appears to be well conserved between DENV3 and DENV2 (Fig. 2D). Restrictions imposed by the length and flexibility of the NS5 interdomain linker must govern the NS5 overall shape. Indeed, we observed previously that altering linker plasticity (by introducing the I265P mutation, using the

TABLE 2 Summary of structure superposition with DENV2 NS5[a]

	DENV2-B			ZIKV			JEV		
NS5 source	*Z* score	RMSD (Å)	No. of α carbons	*Z* score	RMSD (Å)	No. of α carbons	*Z* score	RMSD (Å)	No. of α carbons
DENV2-A	56.7	0.6	873	54.8	2.6	833	50.3	2.5	843
JEV	49.2	2.5	869	57.1	1.0	878			

[a]Superpositions were performed automatically using the Dali server (ekhidna2.biocenter.helsinki.fi/dali/). *Z* scores and RMSD of residual distances between α-carbon atoms following superpositions are indicated. DENV2-A and DENV2-B, DENV2 NS5 protein monomers A and B, respectively (PDB accession number 5ZQK [this work]). The PDB accession number for ZIKV NS5 is 5TFR (monomer A), and the PDB accession number for JEV NS5 is 4K6M (monomer B).

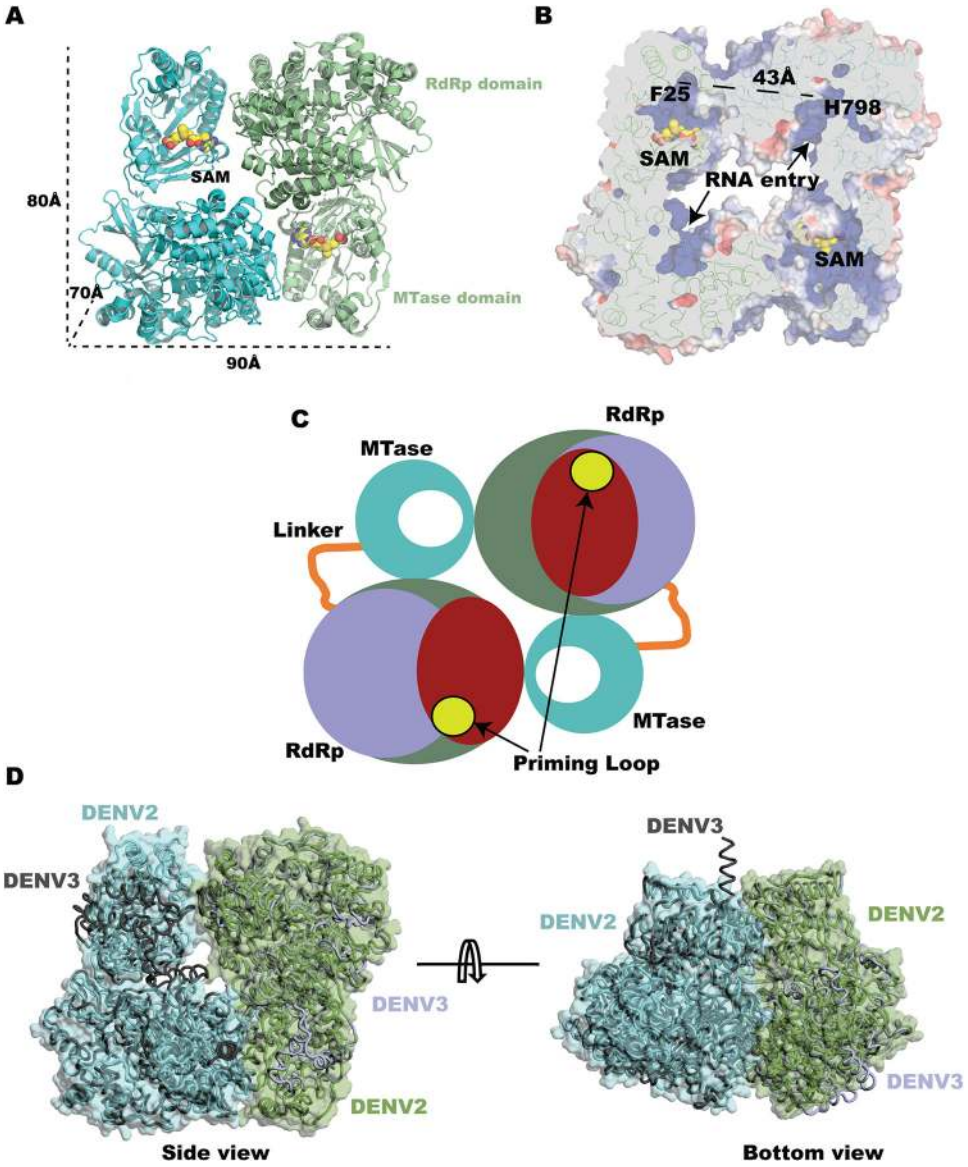

FIG 2 Overall view of the DENV2 NS5 head-to-tail dimer. (A) The two NS5 monomers (colored in cyan and light green, respectively) are represented as ribbons, with α-helices shown as coils and β-strands shown as arrows. The active site of each MTase domain accommodates a SAM cofactor, depicted as yellow and red spheres. The overall dimensions of the dimer are indicated. (B) Electrostatic surface representation of the NS5 crystallographic dimer. Positively charged surfaces are represented in blue, and negatively charged surfaces are represented in red. The distance between F25 in the MTase RNA binding groove and H798 in the priming loop of the RdRp domain of the other monomer is indicated. The RNA template entry sites for each RdRp are indicated by arrows. The α-carbon backbone of each NS5 monomer (colored in cyan and light green) is overlaid. (C) Schematic representation of the DENV2 NS5 dimer showing the relative orientation of subdomains, with the noncrystallographic dyad running perpendicular to the plane of the figure. DENV2 MTase is colored in cyan (the active site is depicted as a white disk), and the RdRp thumb, palm, and fingers subdomains are colored in green, red, and purple, respectively. (D) Superposition (based on the RdRp domains) of two DENV3 NS5 monomers (21), colored gray and light blue, onto the individual DENV2 monomers present in the asymmetric unit (represented by their molecular surfaces, colored in green and blue). The molecular envelope of the present DENV2 dimer can accommodate the closed conformation adopted by the DENV3 NS5 monomer.

numbering for DENV2) abolished DENV2 replication, while changing the linker length attenuated DENV2 growth (31). During evolution of the flavivirus replication complex, intermolecular interactions with other viral or host cell proteins may have further constrained the flavivirus NS5 to remain within a certain molecular volume, and additional restrictions may have been imposed by the linker.

TABLE 3 Amino acid residues involved in DENV2 NS5FL dimeric interface[a]

No.	Interface area (Å²)	Interface location	Residue 1	Residue 2	Interaction, distance (Å)
1	1,037.6	MTase-RdRp (palm)	Ser 152 (OG)	Glu 527 (OE1)	Hydrogen bond, 2.91
		MTase-RdRp (palm)	Arg 161 (NH2)	Gly 528 (O)	Hydrogen bond, 3.19
		RdRp-RdRp (thumb-thumb)	Thr 855 (OG1), (N)	Gly 853 (O)	Hydrogen bond, 3.23, 3.01
2	703.9	RdRp-RdRp (thumb-finger)	Leu 749 (N)	Arg 587 (O)	Hydrogen bond, 3.24
		RdRp-RdRp (thumb-finger)	Arg 750 (N)	Glu 311 (OE2)	Hydrogen bond, 3.90
		RdRp-RdRp (thumb-finger)	Arg 750 (NH1)	Thr 291 (O)	Hydrogen bond, 2.67
		MTase-MTase	Lys 47 (NZ)	Glu 44 (OE2)	Salt bridge, 3.38
		RdRp-RdRp (finger-finger)	Lys 421 (NZ)	Glu 425 (OE1)	Salt bridge, 3.60
3	592.3	MTase-RdRp (finger)	Arg 200 (O)	Tyr 295 (N)	Hydrogen bond, 2.96
		MTase-RdRp (finger)	Gly 227 (N)	Tyr 295 (OH)	Hydrogen bond, 2.82
		MTase-linker	Asn 228 (N)	Glu 269 (OE1)	Hydrogen bond, 3.54
		MTase-linker	Asn 228 (N)	Glu 269 (OE2)	Hydrogen bond, 3.72
4	288.3	MTase-RdRp (finger)	Arg 238 (NH1)	Asp 276 (OD1)	Salt bridge, 2.73
5	118.7	MTase-RdRp (thumb)	Arg 247 (NH1)	Asp 721 (O)	Hydrogen bond, 2.73
		MTase-RdRp (thumb)	Arg 247 (NH2)	Asp 827 (OD2)	Salt bridge, 2.70
6	68.0	MTase-RdRp (thumb)	Arg 200 (NH1)	Asn 877 (OD1)	Hydrogen bond, 3.03

[a]Buried surface area and interface amino acid residues between DENV2 NS5FL monomers were determined using the PISA server (https://www.ebi.ac.uk/pdbe/pisa). Low complex formation significance scores (CSS) were observed for all interface areas determined (value = 0), suggesting that the monomer and monomer form weak contacts in solution. However, in the context of the replication complex where NS5 is sequestered with viral RNA and other viral and host proteins, these amino acid interactions may be important.

The MTase and RdRp domains. Like the DENV MTase domain crystal structures (8, 17), the DENV2 MTase domain (residues 1 to 263) in the full-length protein contains a bound *S*-adenosylmethionine (SAM) cofactor and adopts a similar fold with four helices surrounding a seven-strand β-sheet (Fig. 1A; Table 4). Likewise, the DENV2 RdRp domain in the full-length NS5 structure has a conformation similar to that of isolated

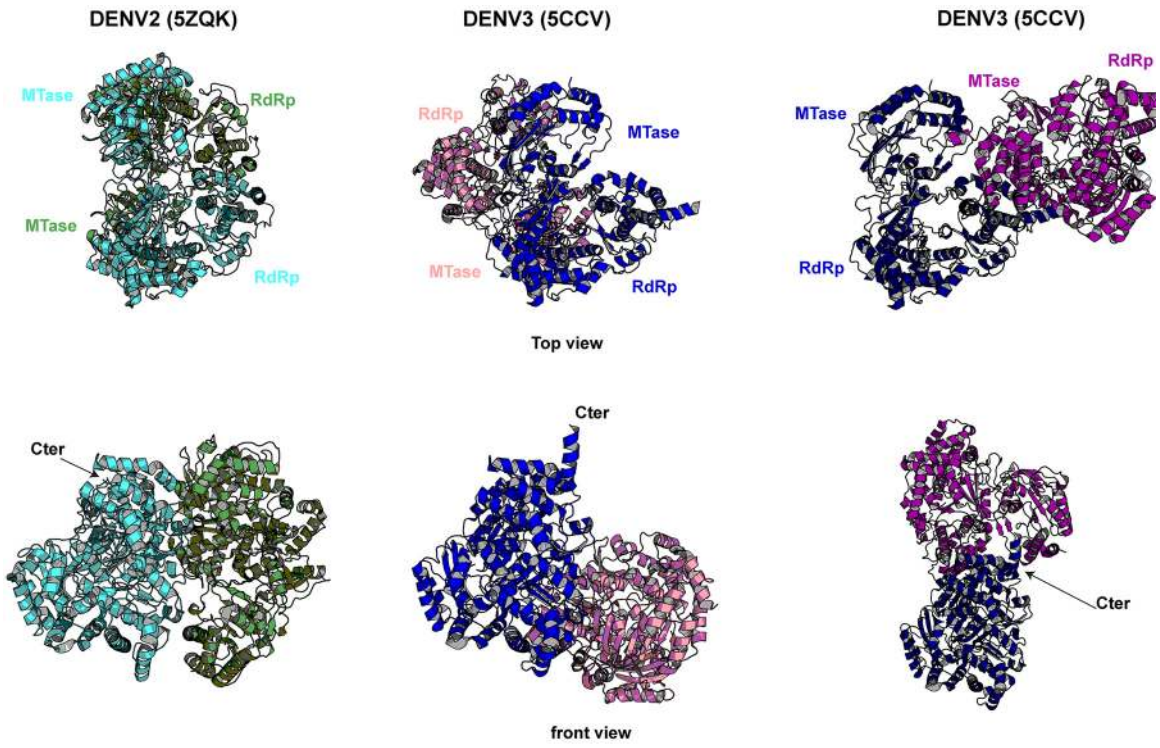

FIG 3 Comparison of DENV2 and DENV3 NS5 dimerization modes. (Top and bottom) Side and top views, respectively, of the interactions between NS5FL monomers. In each panel in the same row, one NS5FL monomer at the front of the figure is displayed in approximately the same orientation. (Left) The DENV2 NS5 dimer (this work), where NS5 monomers are colored in blue and green. (Middle) DENV3 NS5 type I dimers (PDB accession number 5CCV), with molecules A and B colored in pink and blue, respectively. (Right) DENV3 NS5 type II dimers (PDB accession number 5CCV), with molecules A and G colored in violet and purple, respectively. The positions of the RdRp and MTase domains from each monomer are indicated in the top row. The locations of the C-terminal (Cter) ends of the DENV2 and DENV3 monomers are shown in the bottom row.

TABLE 4 Comparison of MTase and RdRp domains in DENV2 NS5FL with known DENV2 and DENV3 MTase and RdRp domain crystal structures

Enzyme and domain (PDB accession no.)	Value for DENV2 NS5FL MTase or RdRp domain			
	RMSD (Å)	*Z* score	No. of superimposed α-carbon atoms	% sequence identity
MTase				
DENV2 NGC (1L9K)	0.7	43.3	261	97
DENV3 (4R8S)	0.6	42.8	256	78
RdRp				
DENV2 NGC (5K5M)	1.9	49.8	573	99
DENV3 (2J7U)	1.8 Å	48.8	557	78

DENV RdRp domain structures (18–20) (Table 4). For the first time, however, RdRp motifs F (residues 452 to 475) and G (residues 406 to 417), which are involved, respectively, in nucleoside triphosphate and RNA template binding (7, 11), are well-ordered in a DENV apo-NS5 structure (Fig. 4A and B). In previous DENV3 NS5 structures, motif F was largely disordered. Residues 470 to 475 form two helical turns at the N terminus of helix α10 in the finger subdomain of DENV3 NS5 (18–20) (Fig. 4C, green). In the present DENV2 NS5 structure, motif F residues 453 to 476 (with residues 464 to 467 being disordered in monomer A) form a β-strand that runs roughly perpendicular to the direction of the now shorter helix α10 (Fig. 4C, red) and contributes a fifth β-strand to the four-strand β-sheet β9a-β2-β3-β1 (Fig. 4C). The same conformation is found for residues 454 to 477 in ZIKV NS5 (24, 25) and residues 455 to 478 in JEV NS5 (26).

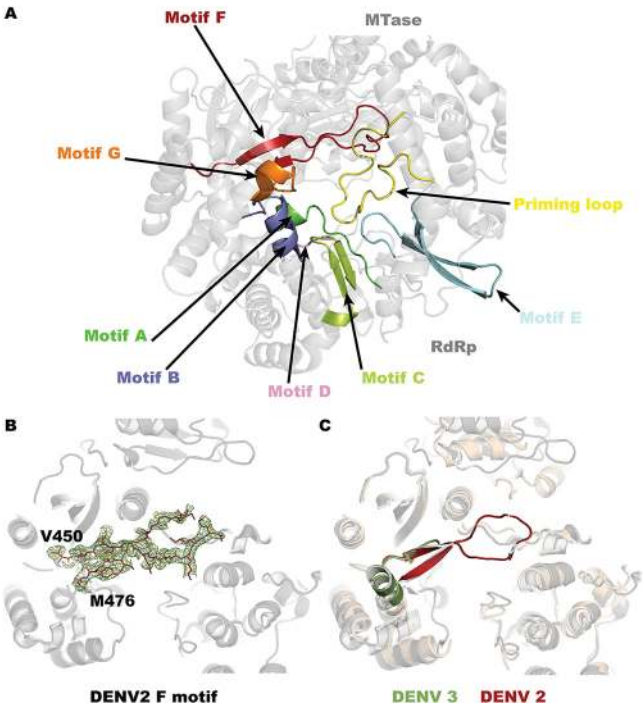

FIG 4 RdRp domain of DENV2 NS5FL. (A) Canonical front view of the RdRp domain in DENV2 NS5, highlighting functional motifs A to G and the priming loop (colored in yellow), which are important for polymerization and RNA recognition. (B) These motifs are well resolved in the electron density, as exemplified by motif F (residues V450 to V476, shown as sticks with the $2F_o - F_c$ electron density map, contoured at a level of 1σ, overlaid). (C) Residues from motif F adopt a conformation in DENV2 RdRp (red ribbons), where they fold into two β-strands connected by a long loop, drastically different from that in DENV3, where they form an α-helix (green ribbons).

Residues 407 to 418, comprising motif G, were also disordered in earlier crystal structures of the DENV2 RdRp domain (20) and the DENV3 RdRp domain and DENV3 NS5 (17–21). Binding of an inhibitor to DENV3 RdRp stabilized its structure (19). In the current DENV2 NS5 structure, residues 407 to 418 are clearly visible and superimpose well with the residues of ZIKV NS5 (24, 25) and JEV NS5 (26) that form the G motif. Thus, motifs F and G can adopt several conformations that may correlate with the interdomain linker conformation and mediate cross talk between the two enzymatic domains. How the conformation of the interdomain linker (compact in DENV3 versus extended in DENV2, ZIKV, and JEV) influences the orientations of the F and G motifs will require further investigation.

Linker and MTase-RdRp interface. Although the length of the NS5 linker (defined here as 9 residues) was preserved during flavivirus evolution, its amino acid sequence is poorly conserved (Fig. 5A). We present in Fig. 5B a structural comparison of the linker region from DENV2 and DENV3 (21), ZIKV (25), and JEV (26) NS5. In JEV NS5, the linker is only partially resolved due to its mobility. The MTase-RdRp interface is significantly smaller for DENV2 NS5 (350 Å^2) than for DENV3 NS5 (677 Å^2), ZIKV NS5 (753 Å^2), or JEV NS5 (599 Å^2). Consequently, fewer amino acid interactions are observed between the DENV2 MTase and RdRp domains. These interactions are also present in the JEV and ZIKV NS5FL structures but are absent in DENV3 (Fig. 6).

To investigate the functional importance of the NS5 linker, we replaced the DENV2 NS5 linker (residues 264 to 272; DENV2 numbering) with the corresponding sequences from DENV1, DENV3, DENV4, ZIKV, or JEV. The enzymatic activities of recombinant DENV2 NS5 wild-type (WT) and mutant proteins (labeled L9) were assayed using established *in vitro* MTase (17, 22, 32, 33) and RdRp (12, 20, 22, 34) biochemical assays (15). Overall, the *in vitro* N-7 and 2′-*O* MTase activities of DENV2 NS5FL were not significantly affected by the introduction of heterotypic linkers (≤2-fold change compared to the WT activity) (Fig. 7A; Table 5). The effects of heterotypic linkers on the *in vitro* DENV2 NS5 *de novo* initiation and elongation polymerization activities were similarly moderate (≤2-fold change compared to the WT activity) (Fig. 7B; Table 6). Using differential scanning fluorimetry, we ascertained that these results were not influenced by differences in the thermostability of the recombinant proteins (0.5°C to 3.5°C variation from the WT) (Table 5).

We further examined the impact of heterotypic NS5 linkers on viral replication by electroporating WT DENV2 (35) and NS5 linker (L9) mutant luciferase reporter replicons into baby hamster kidney fibroblasts (BHK-21 cells) (Fig. 7C). At day 1 postelectroporation, the levels of replication of the mutant DENV2 replicon with DENV1, -3, and -4 NS5 linkers were 2.1, 1.8, and 0.8 log poorer than the level of replication of the WT replicon. On days 2 to 4, DENV1, -3, and -4 L9 mutant replicons grew, respectively, 0.8, 0.5, and 0.2 to 0.5 log slower than the WT. Thus, replacement of the DENV2 NS5 linker with the DENV1, -3, and -4 NS5 linkers did not significantly compromise DENV2 replication in cells. These results are in agreement with the modest impact of heterotypic DENV linkers on the *in vitro* DENV2 NS5 MTase and polymerase activities (Fig. 7A and B). In contrast, the introduction of JEV and ZIKV NS5 linkers abolished the growth of the DENV2 replicon. No luciferase activities were detected during the 4-day study. The replicon results are not easily reconciled with the biochemical data, which showed the preservation of enzymatic activities in JEV and ZIKV L9 mutant NS5 proteins (Fig. 7A and B; Tables 5 and 6). It is therefore likely that, in the context of the viral replication complex, JEV and ZIKV NS5 linkers impede the nonenzymatic functions of the DENV2 NS5FL protein, such as NS5 protein dynamics or the interactions of NS5 with other viral and host proteins that are essential for virus replication. The greater dissimilarity of the ZIKV and JEV linker sequences with those from DENV1 to DENV4 is in line with this hypothesis (Fig. 5A).

Replacing the first four NS5 linker residues (residues 264 to 267) in the DENV2 replicon, corresponding to the 3_{10}-helix in the DENV3 NS5 structure (20–23), with JEV and ZIKV residues (L4 mutants) permitted attenuated growth, albeit at rates lower than

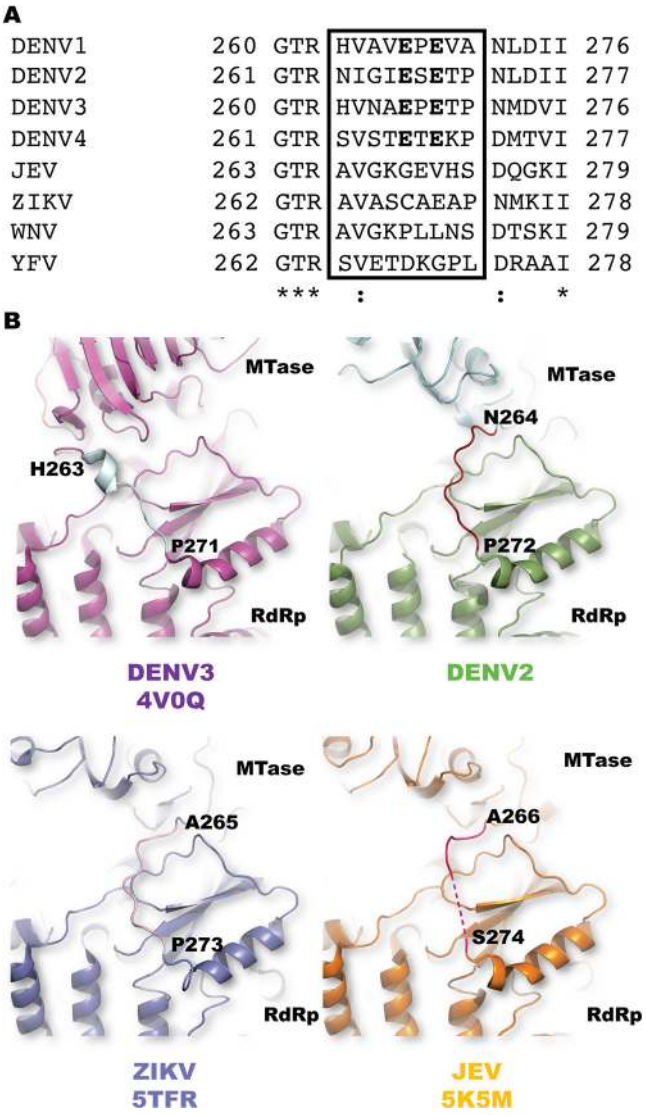

FIG 5 Flavivirus NS5 interdomain linker. (A) Alignment of amino acid residues spanning the flavivirus NS5 interdomain linker from dengue virus serotypes 1 to 4 (DENV1 to DENV4, respectively; GenBank accession numbers ABG75766.1, AES93110.1, EU081206, and ABR13879.1, respectively), yellow fever virus (YFV; GenBank accession number AFH35044), JEV (sequence obtained from PDB accession number 4K6M) (26), West Nile virus (WNV; GenBank accession number AAF20092.2), and ZIKV (GenBank accession number YP_009227205) (25), obtained using the ClustalW program (40). Linker residues inferred from known crystal structures of flavivirus full-length NS5 proteins are boxed. Strictly conserved amino acids are marked with an asterisk below the sequences, and conserved residues are marked with a colon. The two Glu residues conserved in DENV1 to DENV4 linker sequences are in bold. (B) Side-by-side view of the linker structure at the MTase-RdRp interface for the various flavivirus NS5 proteins discussed in the text. The more compact 3_{10}-helix (20–23) leads to a larger interface for DENV3 NS5, while the NS5 proteins from DENV2 (this work), ZIKV (25), and JEV (26) have a more extended linker (partly disordered for JEV), leading to more open structures and smaller interfaces.

those for the DENV-1, -3, and -4 L4 replicon mutants (Fig. 7D). Not surprisingly, heterotypic DENV L4 mutant replicons replicated better than their L9 counterparts, with the DENV4 L4 mutant exhibiting growth kinetics almost similar to those of the DENV2 WT replicon (Fig. 7D). Overall, these data suggest that the first 4 residues from the linker play a less important role than the following residues in modulating NS5 functions. This is in line with earlier work, where increasing the linker flexibility with the I265G substitution generated slightly attenuated viruses, while the I265P substitution, which imposed rigidity in the linker and restricted NS5 dynamics, abolished virus replication (31).

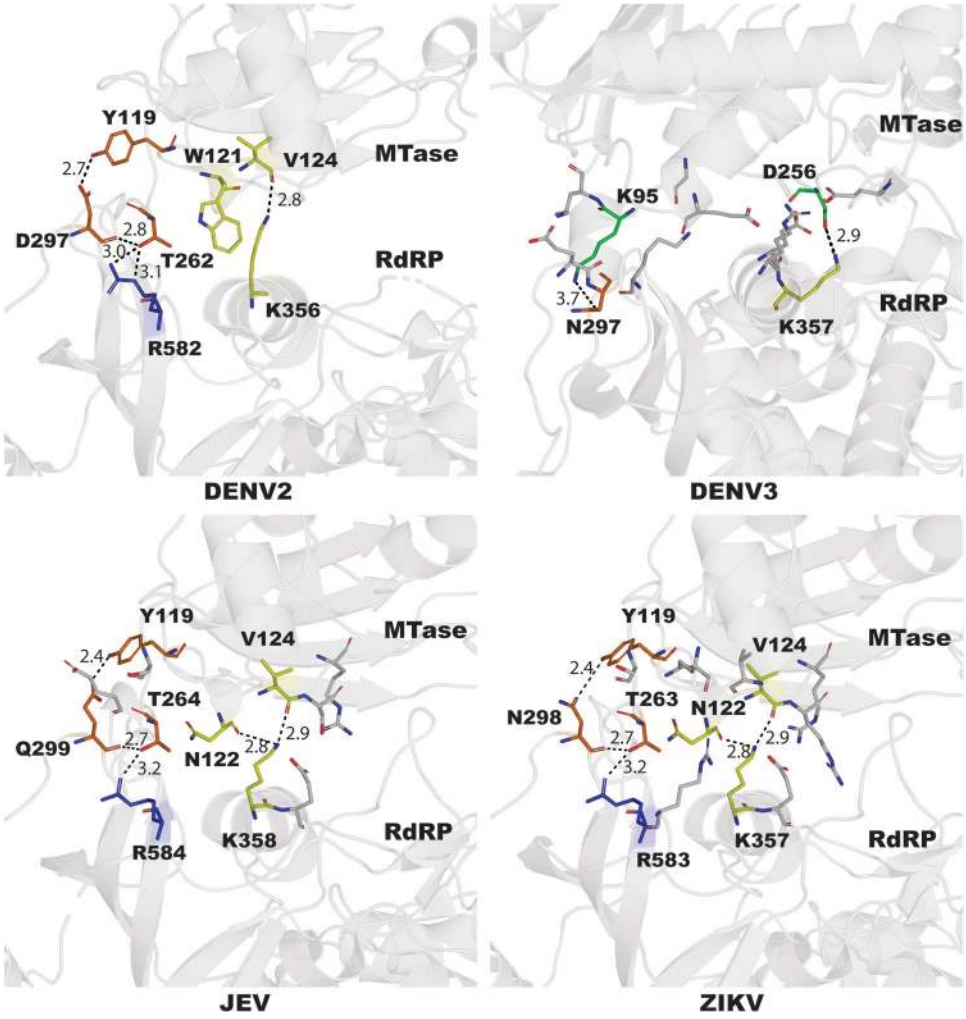

FIG 6 Interactions at the MTase-RdRp interface for various flavivirus NS5FL proteins. The values are extracted from the crystal structures of DENV2 (this work), DENV3 (PDB accession number 4V0Q), JEV (PDB accession number 4K6M), and ZIKV (PDB accession number 5TFR). Interatomic distances between residues are given in angstroms. Residues forming spatially equivalent interactions are shaded with the same color.

In conclusion, we found that the conformation of NS5 from DENV2 resembles the extended conformations adopted by NS5 from JEV and ZIKV rather than the compact form found in DENV3 NS5. This can be attributed to the flexible interdomain linker, which allows NS5 to transition between these and possibly other conformations. While heterotypic DENV NS5 linkers have modest effects on DENV2 NS5 enzymatic activities and virus replication, JEV and ZIKV NS5 linkers abolished DENV2 replication in cells without significantly impacting DENV2 NS5 enzymatic activities. We postulate that the interdomain linker governs critical NS5 dynamics and protein-protein interactions in cells that are essential for virus replication.

MATERIALS AND METHODS

Expression and purification of DENV2 full-length NS5 for crystallization and enzyme assays. The DENV2 WT full-length NS5 coding sequence (Singapore strain; GenBank accession number AES93110.1) was amplified by PCR and inserted into a pNIC28-Bsa4 plasmid by ligation-independent cloning. *Escherichia coli* BL21 competent cells were transformed with the pNIC28a-D2-FL-NS5 plasmid. Cells were grown in LB medium at 37°C until the optical density at 600 nm reached a value of 1. The cells were cooled to 16°C, and protein expression was induced with the addition of 0.1 mM isopropyl-β-D-1-thiogalactopyranoside overnight at 16°C under agitation. Cells were pelleted by centrifugation, and the pellet was resuspended in buffer A (20 mM Na HEPES, pH 7.5, 500 mM NaCl, 10 mM imidazole, 10% [vol/vol] glycerol) supplemented with cOmplete protease inhibitor cocktail (Roche) and DNase. Cell lysis was done by sonication, the debris were removed by centrifugation, and the lysate was injected onto a

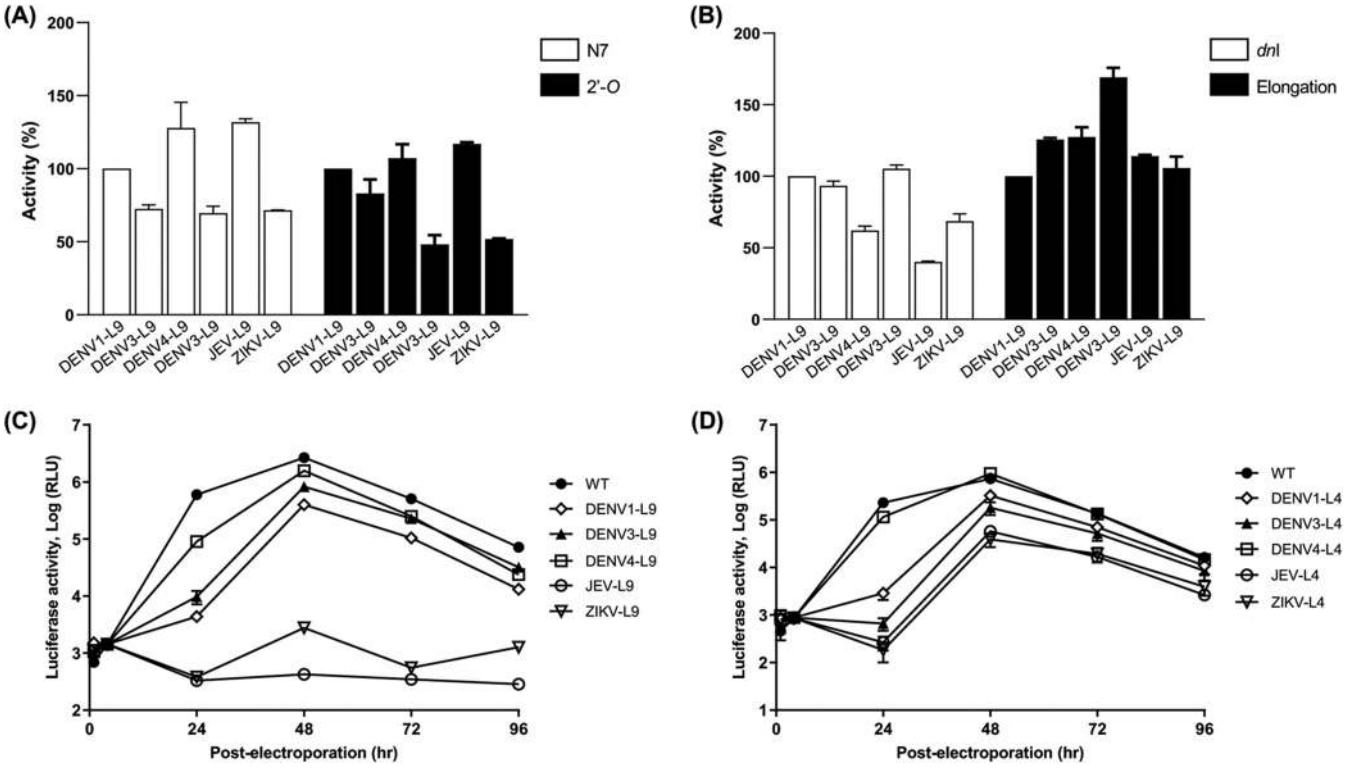

FIG 7 Effects of NS5 linker substitutions on DENV2 NS5 enzymatic activities and growth of the DENV2 replicon. (A and B) *In vitro* N-7 and 2′-*O* MTase activities (A) and RdRp de novo initiation (*dn*I) and elongation activities (B) of DENV2 WT and mutant NS5 proteins in which 9 residues (amino acids 264 to 272; DENV2 numbering) were replaced by DENV-1, DENV3, DENV4, ZIKV, and JEV NS5 linkers. (C and D) Renilla luciferase activities of DENV2 WT and mutant replicons in which 9 residues (amino acids 264 to 272; DENV2 numbering) (C) or 4 residues (amino acids 264 to 267; DENV2 numbering) (D) were replaced by DENV-1, DENV3, DENV4, ZIKV, and JEV NS5 linkers. Equal amounts of WT and mutant replicon RNA were electroporated into BHK-21 cells, and luciferase activities were assayed at the indicated time points over a 4-day period. The *y* axis shows the $\log_{10}$ value of renilla luciferase activity (in relative light units [RLU]). Each data point is the average for two replicates, and error bars show the standard deviations. Each experiment was performed in duplicate.

HisTrap 5-ml column (GE Life Sciences). After a wash step using buffer A supplemented with 40 mM imidazole, the protein was eluted using a gradient of 50 to 500 mM imidazole. The fractions containing the NS5 protein were pooled and dialyzed against 20 mM Na HEPES, 300 mM NaCl, and 10% (vol/vol) glycerol in the presence of tobacco etch virus protease overnight at 4°C. The protein was injected onto a HisTrap 5-ml column (GE Life Sciences) that had been preequilibrated with buffer A to eliminate uncleaved protein and the histidine tag, and the flowthrough was collected. The protein was then diluted to reduce the NaCl concentration from 300 to 50 mM and injected onto a HiTrap heparin affinity column. Protein was eluted using a linear gradient of 50 mM to 1 M NaCl. Fractions containing NS5 were pooled, concentrated, and injected onto a Hi Load S200 16/60 (GE Life Sciences) size exclusion chromatography (SEC) column that had been preequilibrated with 20 mM Na HEPES, pH 7.5, 0.3 M NaCl, 2 mM Tris(2-carboxyethyl)phosphine hydrochloride. Fraction content and purity were checked by SDS-PAGE. The

TABLE 5 *In vitro* N-7 and 2′-*O* MTase activities of DENV2 WT and linker mutant NS5FL proteins[a]

Virus	Activity (%)		Thermofluorescence
	N-7 MTase	2′-*O* MTase	T_m (°C)
WT	100 ± 0	100 ± 0	37.5
DENV1 L9	72.5 ± 2.8	83.1 ± 9.4	39
DENV3 L9	127.9 ± 17.5	107.2 ± 9.6	38
DENV4 L9	69.6 ± 4.6	48.3 ± 6.2	41
JEV L9	131.7 ± 2.3	116.9 ± 1.1	37
ZIKV L9	71.5 ± 0.3	5.9 ± 0.3	37

[a]*In vitro* N-7 and 2′-*O* activities of DENV2 WT and linker (L9) mutant NS5FL proteins were measured with scintillation proximity assays. The results shown are the average percentage of the activity of WT DENV2 NS5FL, derived from two independent experiments, with each data point being determined in triplicate. Thermostability was assessed using the thermodenaturation assay (see Materials and Methods). T_m, melting temperature.

TABLE 6 *In vitro* polymerase activities of DENV2 WT and linker mutant NS5FL proteins[a]

	Activity (%) at the indicated times (h)			
	De novo initiation		Elongation	
Virus	1	2	1	2
WT	100 ± 0	100 ± 0	100 ± 0	100 ± 0
DENV1 L9	93.4 ± 3.2	101.5 ± 4.5	125.5 ± 1.3	127.9 ± 0.7
DENV3 L9	62.0 ± 3.2	61.6 ± 0.0	127.4 ± 6.8	120.8 ± 4.4
DENV4 L9	105.3 ± 2.6	99.0 ± 1.1	169.1 ± 6.7	167.0 ± 2.9
JEV L9	40.0 ± 0.7	35.8 ± 2.4	114.0 ± 0.9	112.4 ± 1.5
ZIKV L9	68.6 ± 5.1	61.5 ± 0.8	105.7 ± 8.1	109.2 ± 5.0

[a]*In vitro* polymerase activities of DENV2 WT and linker mutant NS5FL proteins were measured with *de novo* initiation and elongation fluorescence-based coupled assays. The results shown are the average percentage of the activity of WT DENV2 NS5FL derived from two independent experiments, with each data point being determined in triplicate (see Materials and Methods).

elution volume from the SEC indicated that the protein is eluted as a monomer. Fractions containing NS5 were then pooled and concentrated to 5 mg·ml^{-1} prior to flash freezing at −80°C.

Crystallization and data collection. Crystallization conditions for DENV2 NS5 at a concentration of 3 mg·ml^{-1} were screened using crystallization kits (Molecular Dimensions) and a Mosquito lipidic cubic phase (LCP) nanopipetting robot and the sitting drop technique. The crystals were then manually reproduced and optimized. The mixture for optimized crystallization conditions contained 11 to 15% (wt/vol) polyethylene glycol 4000, 22% (vol/vol) glycerol, 0.1 M Tris HCl at pH 8, and 0.1 M bicine at pH 9 at 4°C with a protein concentration of 5 mg/ml. DENV2 crystals grew within a few days as needles of ~100 μm in length and ~10 μm in width. These needle-shaped crystals had poor diffraction. In order to improve the diffraction quality, the crystals were soaked for 2 months in the precipitant solution. The crystals were then mounted on a cryo-loop and flash frozen in liquid nitrogen. Diffraction data were collected at 100 K at the Proxima 2A microfocus beamline of the SOLEIL Synchrotron (Saint Aubin, France) using an Eiger X 9M detector. Data processing was done using XDS software (36). Data collection statistics are shown in Table 1.

Structure determination and refinement. The crystal structure of the DENV2 NS5 structure was determined by molecular replacement using the PHASER program (37). The search probes were the individual MTase (PDB accession number 3EVG) and RdRP (PDB accession number 5K5M) domain structures. Cell content analysis showed the presence of two molecules in the asymmetric unit. The structure was then refined to a resolution of at 2.3 Å by cycles of manual modification using COOT software (38) and maximum likelihood refinement using the autoNCS and TLS options implemented in the BUSTER-TNT package (39). Refinement statistics are shown in Table 1.

Generation of DENV2 NS5 linker mutant replicons. DENV2 NS5 with chimeric DENV1, DENV3, DENV4, JEV, and ZIKV NS5 linker sequences were generated by overlap PCR. The overlapped PCR products were digested with AccI and PmlI restriction enzymes, followed by cloning into a TA-DENV2 NGC-E shuttle vector (35) at the same sites. The resultant chimeric TA-DENV2 NGC-E shuttle vectors were next digested with BspEI and MluI restriction enzymes and cloned into the pACYC-DENV2 NGC RLUC replicon plasmid using the same sites to generate the DENV2 replicons with chimeric DENV1, DENV3, DENV4, JEV, and ZiKV NS5 linkers. The DENV2 NGC RLUC plasmid contains a T7 promoter and HDVr sequence at its 5′ and 3′ ends, respectively, and the structural genes have been replaced by renilla luciferase (RenLUC) and foot-and-mouth disease virus 2A protease cDNAs (35). All constructs were verified by DNA sequencing.

***In vitro* transcription, RNA transfection, and RenLUC measurements.** DENV2 WT and NS5 linker mutant replicon plasmids were linearized with XbaI followed by *in vitro* transcription (IVT) using a T4 mMessage mMachine kit according to the manufacturer's protocol (Ambion, Austin, TX, USA). IVT RNAs (10 μg) were electroporated into 8×10^6 baby hamster kidney fibroblasts (BHK-21 cells), after which the cells were resuspended in 25 ml Dulbecco modified Eagle medium (Gibco) with 10% fetal bovine serum and 1% penicillin-streptomycin. Cell suspensions of 0.5 ml were seeded into each well of a 12-well plate and kept at 37°C in 5% CO_2. The cells were assayed for luciferase activities at 1, 4, 24, 48, 72, and 96 h posttransfection. Duplicate wells were seeded for each data point. Luciferase assays were performed using a RenLUC assay system following the manufacturer's protocol (Promega, WI, USA).

Generation of DENV2 WT and mutant NS5 proteins. A DENV2 WT NS5 expression plasmid was constructed by PCR amplification of the DENV2 NS5 cDNA from the TA-DENV2 NGC-E shuttle vector (35), followed by digestion with NheI and XhoI and cloning into pET28a vector (Stratagene). To generate pET28a-DENV2 NS5 linker mutant plasmids, chimeric TA-DENV2 NGC-E shuttle plasmids were digested with StuI and PmlI and cloned into the pET28a-DENV2 FL NS5 plasmid. Protein expression and stability were analyzed by thermofluorescence, as described previously (12, 20, 22).

DENV NS5 polymerization assays. The *dn*I/elongation assay was described previously (12, 20, 22, 34). Briefly, the assay reaction mixture comprised 100 nM DENV2 NS5, 100 nM *in vitro*-transcribed DENV2 5′ untranslated region (UTR)-3′ UTR RNA, 20 μM ATP, 20 μM GTP, 20 μM UTP, and 5 μM Atto-CTP (TriLink Biotechnologies) in 15 μl of the assay buffer, comprising 50 mM Tris-HCl at pH 7.5, 10 mM KCl, 1 mM $MgCl_2$, 0.3 mM $MnCl_2$, 0.001% Triton X-100, and 10 μM cysteine. The RNA products generated are mainly from *de novo* initiation, with low levels of terminal nucleotidyltransferase-generated products being

detected. No foldback elongation RNA products were observed (34). The elongation assay reaction mixture was described previously (20, 22) and comprised 100 nM DENV2 NS5, 100 nM *in vitro*-transcribed heteropolymeric RNA template annealed with four primers (primers C1 [3′-AGTCAGTCAGTCAGTGT-5′], A1 [3′-GTCAGTCAGTCAGTCTC-5′], G1 [3′-TCAGTCAGTCAGTCACA-5′], and U1 [3′-CAGTCAGTCAGTCAGA G-5′]), 2 μM ATP, 2 μM GTP, 2 μM UTP, and 0.5 μM Atto-CTP in 15 μl of the assay buffer, comprising 50 mM Tris-HCl at pH 7.5, 10 mM KCl, 0.5 mM $MnCl_2$, 0.001% Triton X-100, and 10 μM cysteine. Each primer allows RNA synthesis to begin with a different base (A, C, G, or U). The use of all four primers allows the unbiased simultaneous incorporation of all four nucleotides. All reactions were allowed to proceed for up to 2 h at room temperature (RT). At the time points indicated above, 10 μl of 2.5× stop buffer (200 mM NaCl, 25 mM $MgCl_2$, 1.5 M diethanolamine, pH 10; Promega) with 25 nM calf intestinal alkaline phosphatase (CIP; New England Biolabs) was added to the wells to terminate the reactions. The plate was shaken and centrifuged briefly at 1,200 rpm, followed by incubation at RT for 60 min, and read on a Tecan Saffire II microplate reader at maximum excitation and emission wavelengths of 422 nm and 566 nm, respectively. All data points were collected in triplicate wells in 384-well black opaque plates (Corning).

DENV NS5 methyltransferase *in vitro* assays. The DENV N-7 MTase assay mixture contained 25 nM DENV MTase, 240 nM biotinylated GpppA-DENV (nucleotides 1 to 110) IVT RNA, 320 nM [^{3}H-*methyl*]SAM in 50 mM Tris HCl, pH 7.5, 20 mM NaCl, and 0.05% (vol/vol) CHAPS {3-[(3-cholamidopropyl)-dimethylammonio]-1-propanesulfonate} (17, 23, 32). The 2′-*O* assay contained 25 nM DENV MTase, 40 nM GpppA-7-mer RNA (TriLink), 320 nM [^{3}H-*methyl*]SAM in 50 mM Tris HCl, pH 7.5, 10 mM KCl, 2 mM $MgCl_2$, and 0.05% CHAPS (17, 22, 23, 33). Buffer, RNA substrate, and enzyme were first mixed in a single well in 96-well, 1/2 area, white opaque plates (Corning Costar, Acton, MA); the reaction was initiated by the addition of [^{3}H-*methyl*]SAM. The N-7 and 2′-*O* reaction mixtures were incubated at RT for 15 min and 1 h, respectively, and then the reactions were stopped with an equal volume of 2× stop solution (100 mM Tris HCl, pH 7.0, 100 mM EDTA, 600 mM NaCl, 4 mg/ml streptavidin-scintillation proximity assay beads [PerkinElmer], 62.5 μM cold SAM). The plate was shaken at room temperature for 30 min at 750 rpm and centrifuged for 2 min at 1,200 rpm, and [^{3}H]methyl incorporation was measured in a TriLux MicroBeta counter (PerkinElmer) with a counting time of 1 min/well.

Data availability. The PDB accession number of the DENV2 NS5 protein determined in the present study is 5ZQK.

ACKNOWLEDGMENTS

This work was supported by grant NRF20016NRF-CRP001-063 to the J. Lescar lab.

We acknowledge SOLEIL for provision of the synchrotron radiation facilities (proposal 20170003) and thank William Shepard and Martin Savko for expert assistance in using beamline Proxima 2A.

REFERENCES

1. Shepard DS, Undurraga EA, Halasa YA, Stanaway JD. 2016. The global economic burden of dengue: a systematic analysis. Lancet Infect Dis 16:935–941. https://doi.org/10.1016/S1473-3099(16)00146-8.
2. Wikan N, Smith DR. 2016. Zika virus: history of a newly emerging arbovirus. Lancet Infect Dis 16:e119–e126. https://doi.org/10.1016/S1473-3099(16)30010-X.
3. WHO. 2017. Yellow fever—Brazil. https://www.who.int/csr/don/04-april-2017-yellow-fever-brazil/en/.
4. Lindenbach BD, Thiel H-J, Rice CM. 2007. Flaviviridae: the virus and their replication, p 1101–1152. In Knipe DM, Howley PM, Griffin DE, Lamb RA, Martin MA, Roizman B, Straus SE (ed), Fields virology, 5th ed, vol 1. Lippincott William & Wilkins, Philadelphia, PA.
5. Chambers TJ, Hahn CS, Galler R, Rice CM. 1990. Flavivirus genome organization, expression and replication. Annu Rev Microbiol 44:649–688. https://doi.org/10.1146/annurev.mi.44.100190.003245.
6. El Sahili A, Lescar J. 2017. Dengue virus non-structural protein. Viruses 5:E19. https://doi.org/10.3390/v9040091.
7. Davidson AD. 2009. Chapter 2. New insights into flavivirus nonstructural protein 5. Adv Virus Res 74:41–101. https://doi.org/10.1016/S0065-3527(09)74002-3.
8. Egloff MP, Benarroch D, Selisko B, Romette JL, Canard B. 2002. An RNA cap (nucleoside-2′-O-)-methyltransferase in the flavivirus RNA polymerase NS5: crystal structure and functional characterization. EMBO J 21:2757–2768. https://doi.org/10.1093/emboj/21.11.2757.
9. Ray D, Shah A, Tilgner M, Guo Y, Zhao Y, Dong H, Deas TS, Zhou Y, Li H, Shi PY. 2006. West Nile virus 5-cap structure is formed by sequential guanine N-7 and ribose 2′-O methylations by nonstructural protein 5. J Virol 80:8362–8370. https://doi.org/10.1128/JVI.00814-06.
10. Dong H, Chang DC, Hua MH, Lim SP, Chionh YH, Hia F, Lee YH, Kukkaro P, Lok SM, Dedon PC, Shi PY. 2012. 2′-*O* methylation of internal adenosine by flavivirus NS5 methyltransferase. PLoS Pathog 8:e1002642. https://doi.org/10.1371/journal.ppat.1002642.
11. Caillet-Saguy C, Lim SP, Shi P-Y, Lescar J, Bressanelli S. 2014. Polymerases of hepatitis C viruses and flaviviruses: structural and mechanistic insights and drug development. Antiviral Res 105:8–16. https://doi.org/10.1016/j.antiviral.2014.02.006.
12. Lim SP, Koh JHK, Seh CC, Liew CW, Davidson AD, Chua LS, Chandrasekaran R, Cornvik TC, Shi PY, Lescar J. 2013. A crystal structure of the dengue virus non-structural protein 5 (NS5) polymerase delineates interdomain amino acid residues that enhance its thermostability and de novo initiation activities. J Biol Chem 288:31105–31114. https://doi.org/10.1074/jbc.M113.508606.
13. Potisopon S, Priet SS, Collet A, Decroly E, Canard B, Selisko B. 2014. The methyltransferase domain of dengue virus protein NS5 ensures efficient RNA synthesis initiation and elongation by the polymerase domain. Nucleic Acids Res 42:11642–11656. https://doi.org/10.1093/nar/gku666.
14. Lim SP. 2019. Dengue drug discovery: progress, challenges and outlook. Antiviral Res 163:156–178. https://doi.org/10.1016/j.antiviral.2018.12.016.
15. Lim SP, Noble CG, Shi PY. 2015. The dengue virus NS5 protein as a target for drug discovery. Antiviral Res 119:57–67. https://doi.org/10.1016/j.antiviral.2015.04.010.
16. Noble CG, Chen YL, Dong H, Gu F, Lim SP, Schul W, Wang QY, Shi PY. 2010. Strategies for development of dengue virus inhibitors. Antiviral Res 85:450–462. https://doi.org/10.1016/j.antiviral.2009.12.011.
17. Lim SP, Sonntag LS, Noble C, Nilar SH, Ng RH, Zou G, Monaghan P, Chung KY, Dong H, Liu B, Bodenreider C, Lee G, Ding M, Chan WL, Wang G, Jian YL, Chao AT, Lescar J, Yin Z, Vedananda TR, Keller TH, Shi PY. 2011. Small molecule inhibitors that selectively block dengue virus methyltransferase. J Biol Chem 286:6233–6240. https://doi.org/10.1074/jbc.M110.179184.
18. Yap TL, Xu T, Chen Y-L, Malet H, Egloff M-P, Canard B, Vasudevan SG,

Lescar J. 2007. Crystal structure of the dengue virus RNA-dependent RNA polymerase catalytic domain at 1.85-angstrom resolution. J Virol 81:4753–4765. https://doi.org/10.1128/JVI.02283-06.
19. Noble CG, Lim SP, Chen Y-L, Liew CW, Yap L, Lescar J, Shi P-Y. 2013. Conformational flexibility of the dengue virus RNA-dependent RNA polymerase revealed by a complex with an inhibitor. J Virol 87:5291–5295. https://doi.org/10.1128/JVI.00045-13.
20. Lim SP, Noble CG, Seh CC, Soh TS, El Sahili A, Chan GK, Lescar J, Arora R, Benson T, Nilar S, Manjunatha U, Wan KF, Dong H, Xie X, Shi PY, Yokokawa F. 2016. Potent allosteric dengue virus NS5 polymerase inhibitors: mechanism of action and resistance profiling. PLoS Pathog 12:e1005737. https://doi.org/10.1371/journal.ppat.1005737.
21. Klema VJ, Ye M, Hindupur A, Teramoto T, Gottipati K, Padmanabhan R, Choi KH. 2016. Dengue virus nonstructural protein 5 (NS5) assembles into a dimer with a unique methyltransferase and polymerase interface. PLoS Pathog 12:e100545. https://doi.org/10.1371/journal.ppat.1005451.
22. Zhao Y, Soh TS, Zheng J, Chan KWK, Phoo WW, Lee CC, Tay MYF, Swaminathan K, Cornvik TC, Lim SP, Shi P-Y, Lescar J, Vasudevan SG, Luo D. 2015. A crystal structure of the dengue virus NS5 protein reveals a novel inter-domain interface essential for protein flexibility and virus replication. PLoS Pathog 11:e1004682. https://doi.org/10.1371/journal.ppat.1004682.
23. Zhao Y, Soh TS, Lim SP, Chung KY, Swaminathan K, Vasudevan SG, Shi PY, Lescar J, Luo D. 2015. Molecular basis for specific viral RNA recognition and 2′-O-ribose methylation by the dengue virus. Proc Natl Acad Sci U S A 112:14834–14839. https://doi.org/10.1073/pnas.1514978112.
24. Ferrero DS, Ruiz-Arroyo VM, Soler N, Usón I, Guarné A, Verdaguer N. 2019. Supramolecular arrangement of the full-length Zika virus NS5. PLoS Pathog 15:e1007656. https://doi.org/10.1371/journal.ppat.1007656.
25. Upadhyay AK, Cyr M, Longenecker K, Tripathi R, Sun C, Kempf DJ. 2017. Crystal structure of full-length *Zika virus* NS5 protein reveals a conformation similar to *Japanese encephalitis virus* NS5. Acta Crystallogr F Struct Biol Commun 73:116–122. https://doi.org/10.1107/S2053230X17001601.
26. Lu G, Gong P. 2013. Crystal structure of the full-length Japanese encephalitis virus NS5 reveals a conserved methyltransferase-polymerase interface. PLoS Pathog 9:e1003549. https://doi.org/10.1371/journal.ppat.1003549.
27. Bussetta C, Choi KH. 2012. Dengue virus nonstructural protein 5 adopts multiple conformations in solution. Biochemistry 51:5921–5931. https://doi.org/10.1021/bi300406n.
28. Saw WG, Tria G, Grüber A, Subramanian Manimekalai MS, Zhao Y, Chandramohan A, Srinivasan Anand G, Matsui T, Weiss TM, Vasudevan SG, Grüber G. 2015. Structural insight and flexible features of NS5 proteins from all four serotypes of dengue virus in solution. Acta Crystallogr D Biol Crystallogr 71:2309–2327. https://doi.org/10.1107/S1399004715017721.
29. Selisko B, Potisopon S, Agred R, Priet S, Varlet I, Thillier Y, Sallamand C, Debart F, Vasseur JJ, Canard B. 2012. Molecular basis for nucleotide conservation at the ends of the dengue virus genome. PLoS Pathog 8:e1002912. https://doi.org/10.1371/journal.ppat.1002912.
30. Dong H, Ren S, Zhang B, Zhou Y, Puig-Basagoiti F, Li H, Shi PY. 2008. West Nile virus methyltransferase catalyzes two methylations of the viral RNA cap through a substrate-repositioning mechanism. J Virol 82:4295–4307. https://doi.org/10.1128/JVI.02202-07.
31. Zhao Y, Soh TS, Chan KWK, Fung SSY, Swaminathan K, Lim SP, Shi P-Y, Huber T, Lescar J, Luo D, Vasudevan SG. 2015. Flexibility of NS5 methyltransferase-polymerase linker region is essential for dengue virus replication. J Virol 89:10717–10721. https://doi.org/10.1128/JVI.01239-15.
32. Chung KY, Dong H, Chao AT, Shi PY, Lescar J, Lim SP. 2010. Higher catalytic efficiency of N-7-methylation is responsible for processive N-7 and 2′-O methyltransferase activity in dengue virus. Virology 402:52–60. https://doi.org/10.1016/j.virol.2010.03.011.
33. Lim SP, Wen D, Yap TL, Yan CK, Lescar J, Vasudevan SG. 2008. A scintillation proximity assay for dengue virus NS5 2′-O-methyltransferase-kinetic and inhibition analyses. Antiviral Res 80:360–369. https://doi.org/10.1016/j.antiviral.2008.08.005.
34. Niyomrattanakit P, Wan KF, Chung KY, Abas SN, Seh CC, Dong H, Lim CC, Chao AT, Lee CB, Nilar S, Lescar J, Shi PY, Beer D, Lim SP. 2015. Stabilization of dengue virus polymerase in de novo initiation assay provides advantages for compound screening. Antiviral Res 119:36–46. https://doi.org/10.1016/j.antiviral.2015.04.007.
35. Ng CY, Gu F, Phong WY, Chen YL, Lim SP, Davidson A, Vasudevan SG. 2007. Construction and characterization of a stable subgenomic dengue virus type 2 replicon system for antiviral compound and siRNA testing. Antiviral Res 76:222–231. https://doi.org/10.1016/j.antiviral.2007.06.007.
36. Kabsch W. 2010. XDS. Acta Crystallogr D Biol Crystallogr 66:125–132. https://doi.org/10.1107/S0907444909047337.
37. Winn MD, Ballard CC, Cowtan KD, Dodson EJ, Emsley P, Evans PR, Keegan RM, Krissinel EB, Leslie AG, McCoy A, McNicholas SJ, Murshudov GN, Pannu NS, Potterton EA, Powell HR, Read RJ, Vagin A, Wilson KS. 2011. Overview of the CCP4 suite and current developments. Acta Crystallogr D Biol Crystallogr 67:235–242. https://doi.org/10.1107/S0907444910045749.
38. Emsley P, Lohkamp B, Scott WG, Cowtan K. 2010. Features and development of Coot. Acta Crystallogr D Biol Crystallogr 66:486–501. https://doi.org/10.1107/S0907444910007493.
39. Smart OS, Womack TO, Flensburg C, Keller P, Paciorek W, Sharff A, Vonrhein C, Bricogne G. 2012. Exploiting structure similarity in refinement: automated NCS and target-structure restraints in BUSTER. Acta Crystallogr D Biol Crystallogr 68:368–380. https://doi.org/10.1107/S0907444911056058.
40. Larkin MA, Blackshields G, Brown NP, Chenna R, McGettigan PA, McWilliam H, Valentin F, Wallace IM, Wilm A, Lopez R, Thompson JD, Gibson TJ, Higgins DG. 2007. Clustal W and Clustal X version 2.0. Bioinformatics 23:2947–2948. https://doi.org/10.1093/bioinformatics/btm404.